JOURNAL OF OPTOELECTRONICS AND ADVANCED MATERIALS, Vol. 11, No. 12, December 2009, p. 2167 - 2171

Comparative study of EXAFS spectra for close-shell systems

N. ALDEA[a*], S. PINTEA[a], V. REDNIC[a], F. MATEI[b], XIE YANING[c]
[a]*National Institute for Research and Development of Isotopic and Molecular Technologies, P.O. Box 700, Cluj-Napoca 5, Romania*
[b]*University of Agricultural Sciences and Veterinary Medicine, Cluj-Napoca, Calea Manastur 3-5, Romania*
[c]*Beijing Synchrotron Radiation Facilities of Beijing Electron Positron Collider National Laboratory, People's Republic of China*

Many systems of real interest for Extended X Ray Absorption Fine Spectroscopy have closed coordination shells. In this paper we focus on the local structural characteristics of supported nickel catalysts and Fe_3O_4 core-shell nanocomposites. The latter are obtained by the polymerization of a conducting polypyrrole shell around Fe_3O_4 nanoparticles. The local structure of Fe and Ni atoms were determined through Extended X-ray Absorption Fine Structure analysis based on the comparative study of the radial distribution function calculated with the classical fast Fourier transform and the Filon quadrature. The radial distribution function can be efficiently calculated by the fast Fourier transform when the coordination shells are well separated while the Filon quadrature gives remarkable results for close-shell coordination. The present work achieved an adequate comparison between different Fourier transform methods for obtaining very accurate local structure results.

(Received July 5, 2009; accepted November 12, 2009)

Keywords: Closed-shell systems, X-ray spectroscopy; Fourier transform algorithms, Radial distribution function, Numerical analysis.

1. Introduction

The X-ray absorption spectroscopy (XAS) can yield several characteristic of the studied material: the electronic and structural information about the local environment around a specific atomic constituent in the amorphous materials [1-2], the location and chemical state of any catalytic atom on any support [3] and the nanoparticle size of the transition metal oxides [4-5].

The X-ray absorption near edge structure (XANES) method is sensitive to local geometries and electronic structure of atoms that form the nanoparticles. The changes in the coordination geometry and in the oxidation state that occur when the crystallite size decreases and the adsorbed molecules interact with the surface can be extracted from the XANES spectrum.

Extended X-ray absorption fine structure (EXAFS) is a scattering technique in which a core electron ejected by an X-ray photon probes the local environment of the absorbing atom. The ejected photoelectron backscattered by the neighboring atoms located around the absorbing atom interferes constructively with the outgoing electron wave depending on its energy. The energy of the photoelectron is equal to the difference between the X-ray photon energy and a threshold energy associated with the ejection of the electron.

2. Theoretical background

The interference between the outgoing and backscattered electron waves has the effect of modulating the X-ray absorption coefficient. The EXAFS function $\chi(k)$ is defined in terms of the atomic absorption coefficient by:

$$\chi(k) = \frac{\mu(k) - \mu_0(k)}{\mu_0(k)}, \quad (1)$$

where k is the electron wave vector, $\mu(k)$ refers to the absorption by an atom from the material of interest and $\mu_0(k)$ refers to the absorption by a free atom. Theories of EXAFS based on the single scattering approximation of the ejected photoelectron by atoms in immediate vicinity of the absorbing atom give the following expression for $\chi(k)$ [6]:

$$\chi(k) = \sum_j A_j(k) \sin\left[2kr_j + \delta_j(k)\right], \quad (2)$$

where the sum extends over j^{th} coordination shell, r_j is the radial distance from the j^{th} shell and $\delta_j(k)$ is the total phase shift function. The amplitude function $A_j(k)$ is given by:

$$A_j(k) = \left(\frac{N_j}{kr_j^2}\right) F(k, r_j, \pi) \exp\left[2r_j / \lambda_j(k) - k^2\sigma_j^2\right] \quad (3)$$

In this expression N_j is the number of atoms in the j^{th} shell, σ_j is the root means squares deviation of distance about r_j, $F(k,r,\pi)$ is the backscattering amplitude and $\lambda_j(k)$ is the mean free path function for inelastic scattering. The backscattering factor and the phase shift depend on the kind of atom responsible for scattering and its coordination shell [7]. The analysis of EXAFS data for obtaining structural information [N_j, r_j,σ_j, λ (k)] generally proceeds by employing the Fourier transform. The radial structure function (RSF) can be derived from $\chi(k)$. The single shell may be isolated by Fourier transform:

$$\Phi(r) = \int_{-\infty}^{\infty} k^n \chi(k) WF(k) \exp(-2ikr) dk . \quad (4)$$

The EXAFS signal is weighted by k^n ($n=1, 2, 3$) to get the distribution function of atom distances. Different apodization windows $WF(k)$ are available as Gauss or Hanning. For experimental reasons it is not possible to cover the full $(-\infty,+\infty)$ wave vector interval. If we take into consideration Δr and Δk as mesh values for variables r and k and we consider N values of k variable, then between meshes Δr and Δk there is following relation:

$$\Delta r = \frac{1}{N\Delta k} . \quad (5)$$

With these assumptions the general relation for discrete Fourier transform is given by relation:

$$\Phi(n\Delta r) = \Delta k \sum_{m=-N/2}^{N/2-1} h(m\Delta k) \exp\left(-\frac{2\pi imn}{N}\right) , \quad (6)$$

where $h = k^n \chi WF$ and $n = \overline{0, N-1}$. The fast Fourier transform algorithm [8] was developed based on relation (6) and was successfully used in many applications. Advantages and limits of this algorithm are treated in reference [9]. Beside this algorithm we also implemented in our software package a generalized Filon quadrature [10] for direct and inverse Fourier transform calculation. The real and imaginary parts of the Fourier transform are given by the following relations:

$$\int_{x_0}^{k_{2n}} h(k) \cos 2\pi kr dk \approx \Delta k \left[\alpha(2\pi r\Delta k)\left(h_{2n} \sin 2\pi k_{2n} r - h_0 \sin 2\pi k_0 r\right) + \beta(2\pi r\Delta k) C_{2n} + \gamma(2\pi r\Delta k) C_{2n-1}\right], \quad (7)$$

$$\int_{x_0}^{k_{2n}} h(k) \sin 2\pi kr dk \approx \Delta k \left[\alpha(2\pi r\Delta k)\left(h_0 \cos 2\pi k_0 r - h_{2n} \cos 2\pi k_{2n} r\right) + \beta(2\pi r\Delta k) S_{2n} + \gamma(2\pi r\Delta k) S_{2n-1}\right], \quad (8)$$

where

$$C_{2n} = \sum_{i=0}^{n} h_{2i} \cos(2\pi r k_{2i}) - \frac{1}{2}\left[h_{2n} \cos 2\pi r k_{2n} + h_0 \cos 2\pi r k_0\right], \quad C_{2n-1} = \sum_{i=1}^{n} h_{2i-1} \sin 2\pi r k_{2i-1} ,$$

$$S_{2n} = \sum_{i=0}^{n} h_{2i} \sin(2\pi r k_{2i}) - \frac{1}{2}\left[h_{2n} \sin(2\pi r k_{2n}) - h_0 \sin(2\pi r k_0)\right], \quad S_{2n-1} = \sum_{i=1}^{n} h_{2i-1} \sin(2\pi r k_{2i-1})$$

and

$$\alpha(\theta) = \frac{1}{\theta} + \frac{\sin 2\theta}{2\theta^2} - \frac{2\sin^2\theta}{\theta^3}, \beta(\theta) = 2\left(\frac{1+\cos^2\theta}{\theta^2} - \frac{\sin 2\theta}{\theta^3}\right), \gamma(\theta) = 4\left(\frac{\sin\theta}{\theta^3} - \frac{\cos\theta}{\theta^2}\right).$$

If $0 < \theta < 1$, functions α, β and γ can be approximated by:

$$\alpha \approx \frac{2\theta^3}{45} - \frac{2\theta^5}{315} + \frac{2\theta^7}{4725}, \beta \approx \frac{2}{3} + \frac{2\theta^2}{15} - \frac{4\theta^4}{105} + \frac{2\theta^6}{567}, \gamma \approx \frac{4}{3} - \frac{2\theta^2}{15} + \frac{\theta^4}{210} - \frac{\theta^6}{11340} .$$

3. Samples preparation and experimental

The magnetic nanocomposite based on polypyrrole was prepared by the oxidative polymerization of pyrrole in aqueous solution containing an oxidant, ammonium peroxodisulfate and water-based magnetic nanofluid. The nanofluid was prepared by the chemical coprecipitation method to obtain Fe_3O_4 nanoparticles, which were stably dispersed in waterby double-layer sterical stabilization with different surfactants combinations: myristic acid and dodecylbenzensulphonate or lauric acid.

The oxidative polymerization of pyrrole in aqueous solution containing dispersed multi-wall carbon nanotubes and Fe_3O_4 magnetic nanofluid results in the attachment of magnetic nanoparticles on the carbon nanotubes. Coprecipitation at room temperature was used for preparation on supported metal supported.

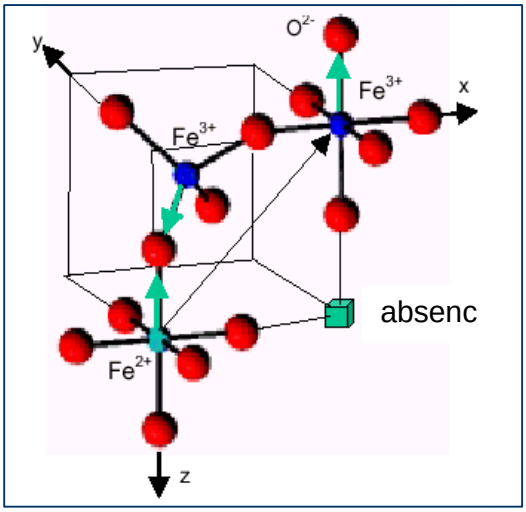

Fig. 1. The unit cell of Fe_3O_4 investigated sample

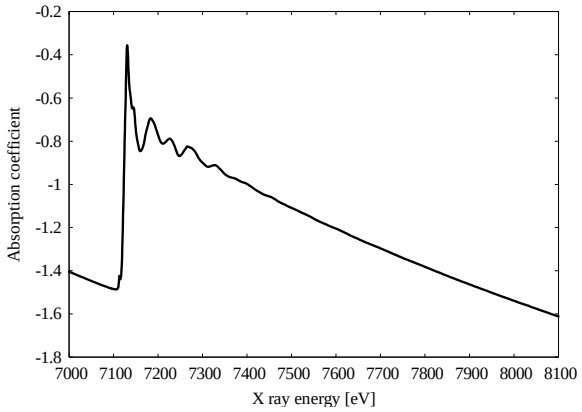

Fig. 2. The absorption coefficients of Fe K edge for investigated sample

The transmission EXAFS measurements were carried out in the *4W1B* beamlines at the Beijing Synchrotron Radiation Facilities (BSRF) operating at 50-80 mA and 2.2 GeV at room temperature. The beamline *4W1B* is an unfocussed monochromatic X-ray beam with 4 mrad of horizontal acceptance. The X-rays are monochromatized by a fixed exit *Si* double crystal monochromator. The features of *4W1B* beamline are: energy range of *3.5-22 KeV*, energy resolution of $\Delta E=0.5\text{-}2$ *eV* at $E=10KeV$, Bragg angle range of $5\text{-}70^0$, the crystals Si(111), Si(220) and Si(311) can be alternatively used. Fe_3O_4 powders with 99.98% purity and Ni nanoclusters supported on Cr_2O_3 treated at 350^0C were used as test samples. Atomic concentration of Ni and Cr were 85 %, respectively 15 at %. Absorption coefficients of Fe and Ni K edges were determined using a Si (111) double-crystal monochromator. Ionization chambers monitored the X-ray intensities of incident and transmitted beams. Harmonics were rejected by detuning of monochromator. Special care was taken in sample preparation, especially for the thickness and homogeneity of the samples, in order to obtain high quality absorption spectra. All samples were ground to fine powder and homogeneously dusted on scotch tape. We used, for absorption coefficients measurements, the energy scanning range from *6994 eV* to *8108 eV* and *8200 eV* to *9300 eV* for Fe_3O_4 and Ni supported on Cr_2O_3, respectively. The EXAFS analysis of the absorption coefficients was processed with computer codes EXAFS51 to EXAFS56 **[**11**]** from our library.

4. Results and discussion

The structure of Fe_3O_4 nanoparticles is an interesting problem from EXAFS perspective because it involves three types of absorbers: the tetrahedral Fe^{3+}, the octahedral Fe^{3+} and octahedral Fe^{2+}. Fig. 1 shows the unit cell of Fe_3O_4 while Figures 2 and 3 show absorption coefficients for Fe and Ni K-edges. The extraction of EXAFS signals requires several steps: calculation of the threshold energy of Fe and Ni K-edges, background removal through pre-edge and after-edge base line fitting with different possible modelling functions, and $\mu_0(k)$ and $\mu(k)$ evaluation. In accordance with Eq. (1) EXAFS signals were processed for intervals 37.5-160 nm^{-1}. and 15.5-161.9 nm^{-1} for Fe_3O_4 and Ni as test samples and are plotted in Figures 4 and 5. In order to obtain the radial structure function (RSF) we use Eq. (4). The mean Fe-O distances of the first and the second coordination shell for standard sample at room temperature are closed to values of R_1=0.189 *nm* and R_2=0.209 *nm.* By taking into account this very small difference between R_1, R_2 and the discrimination steps, Δk and Δr of $\chi(k)$ and $\Phi(r)$ functions given by relation (5), we conclude that it is not possible to obtain a reliable resolution for the RSF. This means that the first and second shells are overlapped or only partial separated. To avoid this disadvantage we developed the Filon algorithm for calculation of the Fourier transform described in relations (7-8). Based on this procedure the Fourier transforms of $k^3\chi(k)WF(k)$ performed in the interval 0.01- 0.5 *nm*, are shown in Fig. 6 for standard Fe_3O_4 powder. Each peak from $|\Phi(r)|$ is shifted from the true distance due to the phase shift function that is included in the EXAFS signal. In the standard sample, the iron ions [Fe^{3+}] and [Fe^{2+}, Fe^{3+}] from tetrahedral and octahedral structure are surrounded by four and six oxygen anions [O^{2-}], respectively. In the EXAFS measured spectra these three contributions are averaged. By analysing Fig. 6 we can observe the advantages of Filon quadrature in comparison with the fast Fourier transform algorithm. The peaks associated with the coordination shells have a high resolution. Another important advantage consists in the large number of point pairs for each peak. This result is very important, for statistical reasons, in the numerical analysis of the coordination number and the radius values of the coordination shells based on the inverse Fourier transform technique. Using this algorithm we obtained for the first and second coordination shells $N_1=3.11\pm0.009$ atoms, $r_1=0.189\pm0.001$ *nm* and $N_2=5.15\pm0.01$ atoms, $r_2=0.209\pm0.001$ *nm*, respectively.

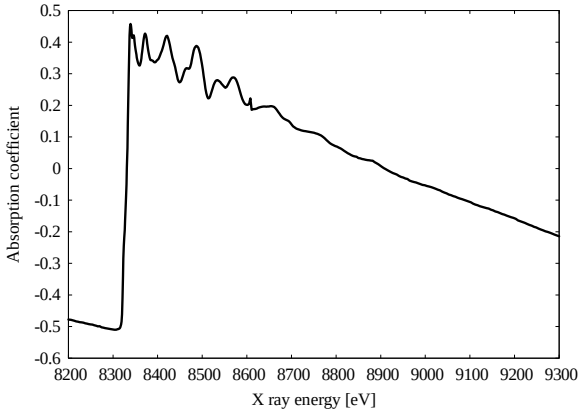

Fig. 3. The absorption coefficients of Ni K edge for investigated sample

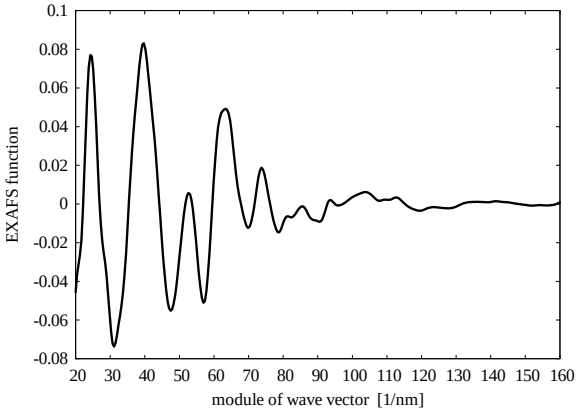

Fig. 4. The EXAFS signal of Fe K edge for investigated sample.

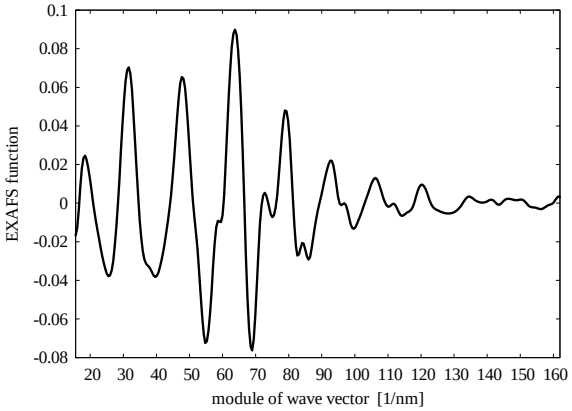

Fig. 5. The EXAFS signal of Ni K edge for investigated sample.

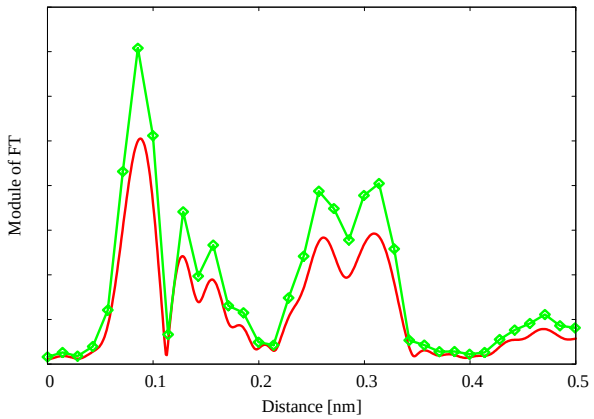

Fig. 6. The Fourier transforms of the EXAFS spectra of Fe_3O_4.system (Filon quadrature – red line), (FFT algorithm – green line and ◊)

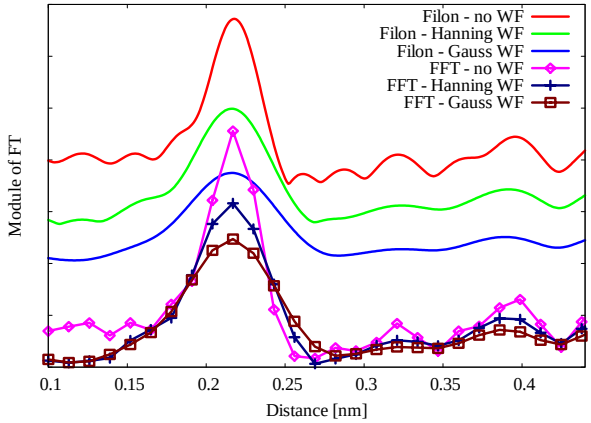

Fig. 7. The Fourier transforms of the EXAFS spectra of supported Ni catalyst calculated by Filon quadrature and FFT algorithm

The Fast Fourier transform method gives poor results when analysing the closed coordination shells because the peaks of the radial structure function from Fig. 6 have a poor resolution. Therefore they can not be used in the calculation of the local structure parameters for systems that have closed coordination shells. They contain one or more types of atoms distributed at two or more unique distances differing by 0.05 *nm* or less. Generally speaking such subshells are not resolved in the fast Fourier transform of the EXAFS spectra and can not be analyzed by Fourier filtering technique. Other methods such as the regularization and the beat methods [12-14] in combination with the fast Fourier transform of RSF are reported in literature. The results based on the last methods are more or less reliable. As comparison Fig. 7 shows the radial distribution function for Ni supported on Cr_2O_3 nanocrystallites calculated by both Filon quadrature and fast Fourier transform algorithms. Because the first and the second coordination shells are not closed, R_1=*0.2491 nm* and R_2=*0.3524 nm*, they can be well separated by both algorithms. By using the similar procedure for the local

structural parameters we obtained $N_1=9.32\pm0.11$ atoms, $r_1=0.25\pm0.06$ *nm*, $N_2=4.46\pm0.02$ atoms, $r_2=0.352\pm0.01$ *nm*, respectively. The contribution of the window functions for each algorithm is also presented in Fig. 7. Various type of windows functions such as Hanning or Gaussian reduce the spurious errors due to integral truncation but they involve a broadening for each contribution.

5. Conclusions

In the present paper we showed how various Fourier transform algorithms with their specific advantages apply to EXAFS analysis and what extra information can they add to understanding the nanostructure of the magnetite surrounded by polypyrrole shell and supported nickel catalysts. The following conclusions can be drawn from these studies:

(i) Filon quadrature can be successfully used for the determination of the structure of closed-shell systems as magnetite while the fast Fourier transform algorithms gives unreliable results for these cases;

(ii) The classical fast Fourier transform method gives good results when the investigated samples are not closed-shell systems as supported metal catalysts.

References

[1] F.W. Lytle, D.E. Sayers, E.A. Stern, Physica B **158**, 701 (1989).
[2] E. A. Stern, X-Ray Absorption: Principles, Applications, Techniques of EXAFS, SEXAFS and XANES, Wiley, New York 1988.
[3] J. H. Sinfelt, G. H. Via, F. W. Lytle, Catal Rev. Sci. Eng. **26**(1), 81 (1984).
[4] L. X. Chen, T.Liu, M. C. Thurnauer, R. Csencsits, T. Rajh, J. Phys. Chem. B **106**,8539 (2002).
[5] R. Turcu, Al. Darabont, A. Nan, N. Aldea, D. Macovei, D. Bica, L. Vekas, O. Pana, M. L. Soran, A. A. Koos, L. P. Biro, J. Optoelectron. Adv. Mater. **8(2)**, 643 (2006).
[6] N. Aldea, A. Gluhoi, P. Marginean, C. Cosma, Xie Yaning, Spectrochim. Acta B **55**, 997 (2000).
[7] A. G. McKale, B. W. Veal, A. P. Paulikas, S. K.Chan, G. S. Knapp, J Am. Chem. Soc. **110**, 3763 (1988).
[8] E. O. Brigham, The Fast Fourier Transform, Prentice-Hall Inc., Englewood Clifs, New Jersy, 1974.
[9] J. S. Walker, Fast Fourier Transform, 3nd edn., CRC Boca Raton, New York London, Tokyo, (1997)
[10] M Abramowich, A. Stegun, Handbook of Mathematical Functions, Dover, New York, 1968.
[11] N. Aldea, E. Indrea, Comput. Phys. Commun. **60**, 145, (1990).
[12] Yu. Babanov, S. Kiryanov, L. Romashev, D. Vyalich, S. Molodtkov, G. Guentherodt, U. Ruediger, Yu. Detkov, M. Fonine, K. Baberschke, H. Wende and Y. U. Idzerda, Physica Scripta **T115**, 194, (2005).
[13] B. I. Bayanov, G. Bunker, T. I. Morrison, J. Synchrotron Rad. **3**, 120 (1966)
[14] S. J. Gurman, J. Synchrotron Rad. **2**, 56 (1995)

*Corresponding author: naldea@itim-cj.ro